Characterization of Octapole Lamp Furnace for in situ High Temperature Ceramic Characterization Techniques

By

ALEJANDRO URDANETA-CARRERA

THESIS

Submitted in partial satisfaction of the requirements for the degree of

MASTER OF SCIENCE

in

Materials Science and Engineering

in the

OFFICE OF GRADUATE STUDIES

of the

UNIVERSITY OF CALIFORNIA

DAVIS

Approved:

_____

Scott J. McCormack, Chair

_____

Jason White

_____

Sabyasachi Sen

Committee in Charge

2025

Abstract

Characterization of materials utilizing *in situ* experimentation techniques is critical for understanding the nature of materials in those conditions. The processing of polymer derived ceramics from pyrolyzing polymer precursors is especially important for understanding the change in their microstructure and material properties as they pyrolyze and form a ceramic material. In this thesis, an octapole lamp furnace (OLF) is characterized for the heat treatment of samples in an open and inert-gas environment. The heat is generated by tungsten-filament halogen lamps that are focused into the center of the furnace. This furnace was constructed to be coupled with X-ray characterization techniques, particularly micro-computed tomography, for *in situ* high temperature characterization. Investigating the capabilities of the OLF culminated in determining the temperatures the furnace reach up to maximum operating power as well as the temperature gradients occurring inside of the furnace. A preceramic polymer, polycarbosilane SMP-10, was pyrolyzed in the furnace to assess its capabilities for pyrolysis experiments. Temperature measurements were made using thermocouples, and ceramic samples were prepared and melted in the furnace for further assessing the OLF capabilities. The thermocouple-determined maximum temperature of the furnace was 1504±23 °C, and highest melting point sample melted in the furnace was $BaTiO_3$ (MP: 1625 °C). The temperature gradient results determined that the hottest spot in the furnace is ~3 mm in each Cartesian x-y-z direction with respect to the geometric center of the OLF. Pyrolysis experiments determined that the OLF is capable of pyrolyzing SMP-10 with a sufficient ramp rate that does not induce thermal shock of the samples. These results demonstrate the OLFs heating capabilities as well as its feasibility for pyrolyzing materials such that it is capable for use in *in situ* high temperature characterization in air and in inert environments.

Acknowledgements

First, I want to thank Professor Scott J. McCormack for being an amazing advisor and inspiring researcher. I have appreciated his insight and guidance throughout my work, and he has challenged the way I think about research for my betterment. I'm grateful for learning from and working with him.

Next, thank you to my committee – Professor Jason White and Professor Sabyasachi Sen, and the other chemical engineering and materials science & engineering faculty who have educated and guided me during this program.

I would like to thank the National GEM Consortium, my incredible mentor Jeremy Feaster, and Mark Mitchell & Dr. Teresa Bear for supporting and providing me with opportunities that I will always cherish.

Thank you to all my fellow members of the McCormack group – Kenny, Randi, Stuart, Will, Nicki, Bryce, and Andreas for their wisdom and support during my research for this thesis.

I also want to thank the friends I made during this program – especially Cun Shuo, Thai, and Paulina who I have had the pleasure of getting to know and have kept me sane during this program.

Finally, I would like to thank my family – my father Alejandro J. Urdaneta, my mother Nancy Urdaneta, and my siblings Gabriela, Alfonso, and Daniel Urdaneta-Carrera for their love and support.

Table of Contents

Chapter 1: Introduction

1.1: Introductory Statement

Understanding how the structure and properties of materials, particularly ceramic materials, changes with increasing temperature is important to understanding how these materials would operate in high temperature applications. This type of temperature-varying data can be obtained with *in situ* experimentation. Designing a furnace that can be incorporated into these *in situ* experiments is the crucial point for obtaining this data. Characterization/imaging techniques such as X-ray computed microtomography (μ-CT) and X-ray diffraction (XRD) are ideal methods for *in situ* experimentation as they involve X-rays passing through a sample and hitting a detector away from the sample. A light source is sufficient to heat while allowing x-rays to pass through the center of the furnace as seen in **Figure 1** below.

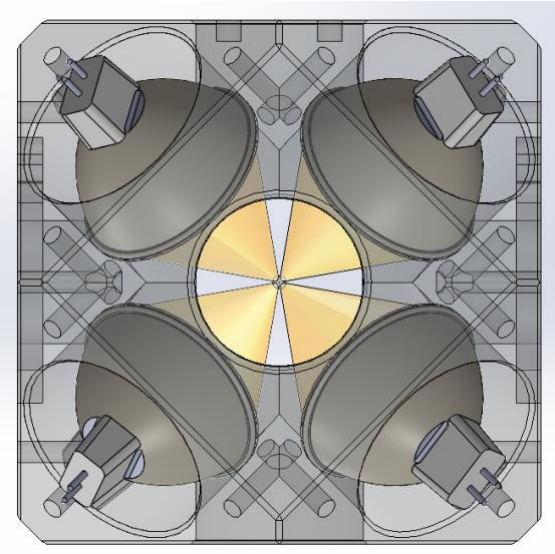

Figure 1*: Open lamp furnace design CAD schematic (side-view) [1].*

In **Figure 1**, the yellow conical sections represent the radiation focused on the center of the furnace, and the open circle in the center represents the windows that allow X-ray beams to propagate to the sample unimpeded. Lamp furnaces have been developed to be coupled with μ-CT and XRD experiments and demonstrated to reach temperatures above 1500 °C [2][3]. These lamp furnaces are equipped to bombard samples with mostly visible-light and infrared radiation as the source of heating.

An octapole lamp furnace (OLF) was designed and manufactured by Tanaka et al. [1] in which eight tungsten-filament halogen optical lamps are used for heating. This work is focused on characterizing and validating the capabilities of this OLF. The OLF was designed and built with the intention of being coupled with μ-CT imaging via a synchrotron source [1]. μ-CT is a powerful technique for high resolution 2D/3D microstructure imaging that is well suited for *in situ* experiments.

The lamps used in the OLF emit ultraviolet, visible, and mostly infrared radiation. The lamps are fixed into the furnace in a way such that their working distances (aka focal lengths) are aligned onto the center of the furnace denoted as the hot spot where the highest heat flux occurs (and presumably where the highest temperature within the furnace occurs). The lamp's radiation is focused on the center of the furnace by a reflective gold coating surrounding the bulb of the lamp. Each of the six square-shaped sides of the furnace has a circular window ranging from 1-2 inches in diameter for open access to the center of the furnace just as depicted in **Figure 1**. These aspects of the OLF culminate in the potential for easily accessing the center of the furnace as well as observing the heating process from outside of the furnace.

1.2: Thesis Objectives

The core objective of this thesis is to assess the capabilities of an existing octapole lamp furnace (OLF) to pyrolyze polymer derived ceramics. To achieve this, the following questions were investigated:

1. Can the OLF effectively heat samples that require low heating ramp rates to prevent thermal shock?
2. Can the OLF pyrolyze polymer derived ceramic samples using an inert-gas environment chamber?

This necessitates answering the following technical questions:

1. What is the OLF's maximum temperature?
2. What is the size of the OLF's hot spot?

These questions are addressed primarily by measuring the temperature in the furnace as well as melting prepared samples in the furnace as proof of reaching their melting point temperature. Testing the pyrolysis of polymer derived ceramics that are susceptible to thermal shock in the OLF will directly address questions 1 & 2. Identifying and developing a reasonable understanding of the phenomena associated with the OLF, such as heat transfer, electrical heating, and thermodynamics, is crucial for the basis of beginning to answer the questions posed.

1.3: Thesis Outline

Chapter 1: Introduction: This chapter highlights the motivation of characterizing the octapole lamp furnace for use in *in situ* experimentation. The main thesis objectives/questions are outlined clearly as metrics for characterizing the furnace.

Chapter 2: Polymer Derived Ceramics: This chapter explains the process of polymer conversion into ceramic materials as well as the importance of characterizing their material properties (i.e., density) as a function of temperature.

Chapter 3: Lamp Furnace Literature Review: This chapter delves into the phenomena associated with the lamps powering the OLF including heat transfer via radiation, interactions between material surfaces and radiation, previous lamp furnace designs, and more.

Chapter 4: Sample Preparation for OLF Characterization: This chapter explains the methodology of the preparation of samples and use of the inert-gas chamber for pyrolysis experiments in the OLF.

Chapter 5: Octapole Lamp Furnace Characterization: Focuses on the investigation of the OLF heating capabilities. This includes the methodology used, results of the experiments, and discussion of the phenomena observed.

Chapter 6: Pyrolysis Experiments for in situ μ-CT: This chapter covers the work done to determine the reliability of the OLF for *in situ* pyrolysis experiments.

Chapter 7: Conclusion and Future Work: This chapter summarizes the main findings from the work showcased in this thesis and how they address the thesis objectives. Additionally, suggestions are made to further support these findings experimentally.

Appendix: This section showcases additional figures not essential to include in their entirety for the main text of the thesis. Data based on unreliable pyrometer measurements and phase diagrams referenced for sample preparation are included.

Chapter 2: Polymer Derived Ceramics

This chapter introduces polymer derived ceramics and describes their processing/synthesis methods. The motivation of using these materials in the OLF for *in situ* experiments is also discussed.

2.1: Pyrolytic Conversion of Polymer to Ceramic

Polymer derived ceramics (PDC) are ceramic materials that were processed from pyrolyzing preceramic polymer precursors. Most PDCs involve silicon carbide, boride, nitride, and oxide bonds as depicted in **Figure 2**.

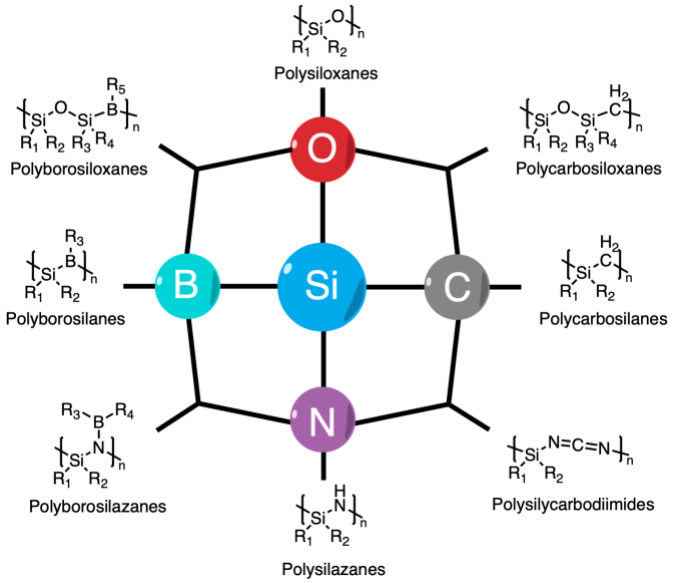

***Figure 2**: Preceramic organosilicon polymer families (R represents carbon groups) [7].*

The process of pyrolyzing the precursors showcased involves off-gassing the H and R (usually aliphatic or aromatic organic side groups) species, leaving the desired Si-(C, B, N, O) backbone structure that makes up the ceramic material. The conversion process that produces PDCs is illustrated in **Figure 3**.

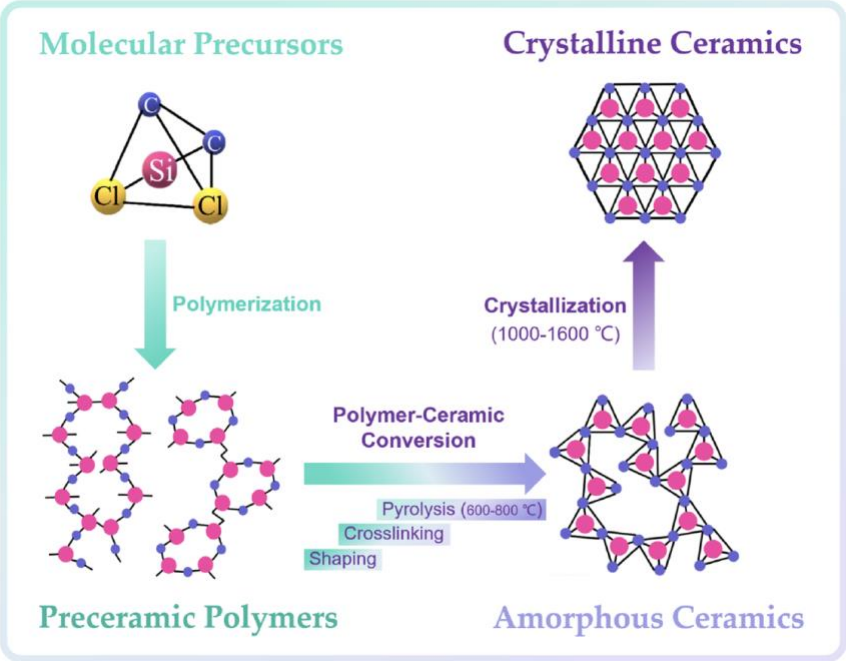

***Figure 3**: Preceramic to ceramic conversion process [8].*

After pyrolysis, the resulting structure is typically amorphous and crystallizes with further heat treatment (although some PDCs can remain amorphous even with additional heat treatment). This crystallization process occurs at much higher temperatures than where pyrolysis occurs.

2.2: Microstructure & Material Properties of PDCs

PDCs have unique microstructures because their synthesis/processing can result in different structural forms [8]. This unique microstructure impacts the material's properties including density, mechanical strength, resistance to wear, etc. Understanding how the microstructure of PDCs change with increasing temperature is important to understanding how these materials would operate in high temperature applications. The OLF coupled with imaging techniques like μ-CT provides quantitative data on how the density of the preceramic polymer changes with temperature as it converts to a ceramic.

Chapter 3: Lamp Furnace Literature Review

In this chapter, relevant phenomena concerning radiation that the lamps used in the lamp furnace emit are described in detail. Additionally, previous studies of lamp furnaces for *in situ* experimentation are briefly showcased along with characteristic results for each lamp furnace design. Finally, the design of the OLF utilized in this work is explained in detail pertinent to the characterization of the heating region of the furnace as well as the application for μ-CT imaging of PDCs.

3.1: Source of Heat: Incandescent Radiation

The lamps in the OLF transfer heat via radiation towards the center of the furnace. Radiation transfers heat through electromagnetic waves. These waves propagate through space (vacuum included), and when the waves are absorbed by an object (generally by electron-state excitation), the object "heats up" and can also be capable of emitting radiation via the excited electron-state releasing a photon to convert back to its ground state configuration [6]. The source of this radiation in the OLF comes from tungsten filament in the bulb of the lamp being heated to temperatures where light is emitted by resistance heating in an electrical circuit. The tungsten filament emits radiation via incandescence, and although it is not a blackbody (the ideal emitter) its emission spectra can be compared to one as a reference for ideal behavior [10]. The nature of its radiation spectra as a function of wavelength can be described by Planck's law of radiation as shown in **Equation 1**.

$$E_\lambda = \frac{8\pi hc}{\lambda^5(exp(hc/\lambda k_b T) - 1)}$$

***Equation 1**: The spectral radiation energy density (E_λ) is dependant on Planck's constant (h), the speed of light (c), the wavelength of radiation (λ), Boltzmann's constant (k_b), and temperature (T).*

However, **Equation 1** just provides reasonable insight into the radiation emitted by an object. It is not a perfect representation of the tungsten filament's behavior when heated, but it does provide valuable insight into the type of radiation emitted. The spectral radiation energy density was normalized to its maximum value and plotted in **Figure 4** below at relevant operating temperatures of the tungsten filament in the lamp.

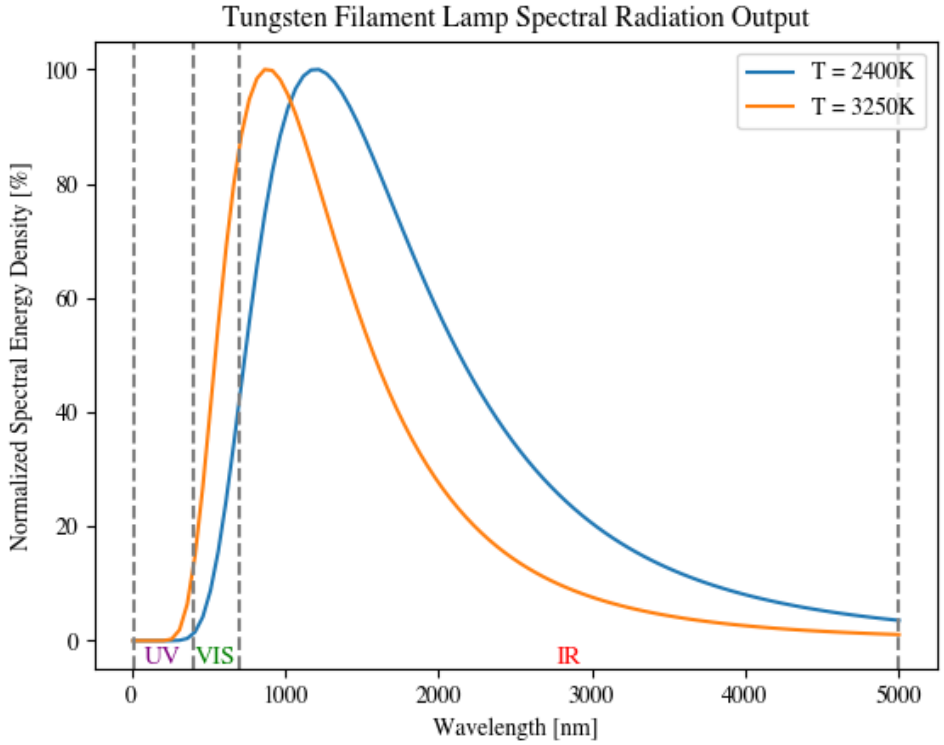

***Figure 4**: Normalized spectral radiation energy density of a blackbody emitter at relevant operating temperatures (3250 K being the maximum operating temperature of the lamp [11]).*

In **Figure 4** most of the radiation emitted lies in the infrared (IR) spectrum, and as the temperature increases more ultraviolet (UV) and visible (VIS) light is emitted. The curves also better indicate

the relative density of different wavelengths being emitted. The peak/maximum wavelengths emitted can be determined by Wien's displacement law by integrating the spectral radiation energy equation with respect to wavelength and solving for the trivial solution, which results in **Equation 2**.

$$\lambda_{max} T = C_w$$

Equation 2*: The product of the max wavelength of light emitted (λ_{max}) and temperature (T) equals a constant (C_w = 2898 μm-K) [6].*

Based on **Equation 2** and the spectral radiation energy distribution shown in **Figure 4**, the most apparent wavelengths emitted (where the curves reach 100%) are at 1208 nm and 892 nm for the temperatures 2400 K and 3250 K, respectively. These findings suggest that the tungsten filament lamps are sufficient for heating objects that absorb visible and infrared radiation while the lamps maintain their operating temperature.

Quantifying how much energy the lamps emit as radiation is useful for determining the amount of energy being radiated into the furnace. Stefan-Boltzmann's law describes the amount of energy emitted by an object as a function of its temperature as shown in **Equation 3**.

$$\frac{P}{A} = \varepsilon \sigma T^4$$

Equation 3*: The power emitted (P) per surface area of the material (A) is dependent on the emissivity of the material (ε), Stefan-Boltzmann's constant (σ), and the temperature of the material (T).*

Emissivity describes the ability of a surface of a material to emit radiation. It is defined as a ratio of the energy radiated by the material to the energy radiated by a blackbody emitter [6]. By this definition, emissivity ranges from zero to one. An emissivity value of zero describes the surface

as a perfect reflector, and an emissivity value of one describes the surface as a blackbody (the perfect emitter). The effect of an inaccurate emissivity value is usually significant when it is a multiplicative factor as in Stefan-Boltzmann's law. Emissivity is dependent on the type of material, the geometry of its surface, as well as the temperature of the material. Different types of emissivity are distinguished because of the multiple terms influencing them, but the simplest form is the total, hemispherical emissivity that is a representative average emissivity over all possible directions and wavelengths. Ideal and real emission behavior is showcased in **Figure 5**.

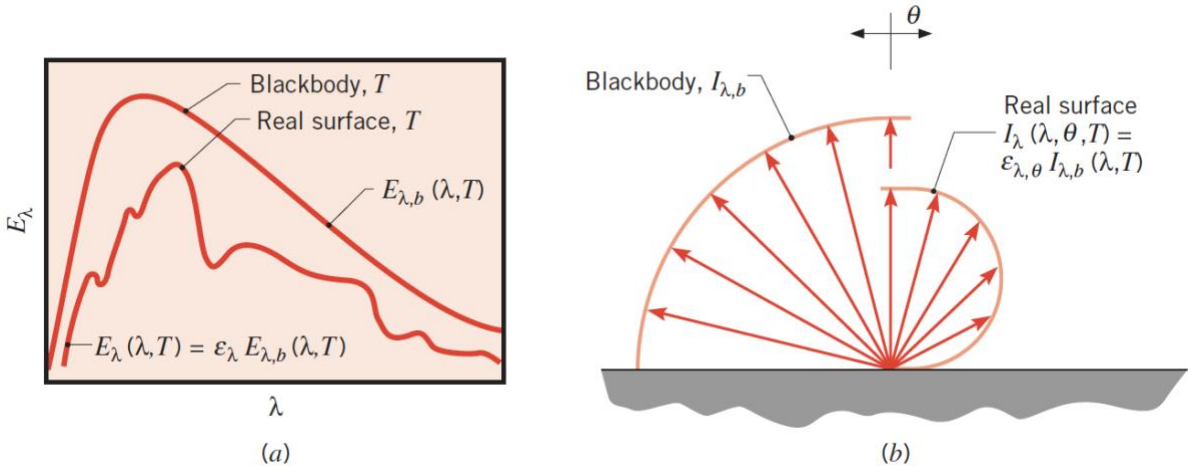

Figure 5*: Comparison of blackbody and real surface emission. (a) Spectral distribution. (b) Directional distribution [6].*

In **Figure 5**, the non-ideal behavior of real surfaces is apparent by the spectral energy distribution (E_λ) and directional intensity distribution (I_λ) being less than their respective blackbody distributions. Emissivity can be viewed as the non-ideality of the real surface.

The spectral emissivity of tungsten filament at different temperatures from the work of Dmitriev V. et al and Izarra C. et al. is shown in **Figure 6** [12][13].

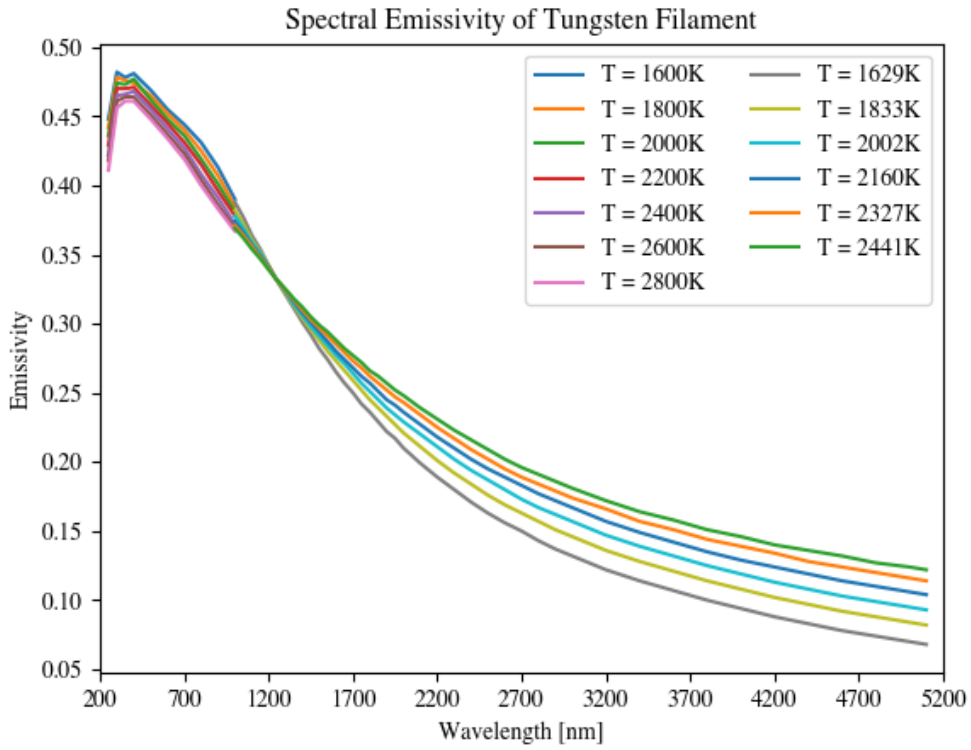

***Figure 6**: Emissivity of tungsten filament as a function of wavelength at specific temperatures. Note that data from λ=250-1000 nm corresponds to one data set and the data from λ=1000-5100 nm corresponds to another data set [12][13].*

In **Figure 6**, there is an increase in emissivity up until ~500 nm where the values start to decrease consistently. The emissivity values decrease with increasing temperature until ~1300 nm where the behavior switches. From this observation it seems that visible-light emissivity decreases with temperature and infrared emissivity increases with temperature. However, it is important to point out that these emissivity values are measured from sources not replicated in this work, so they only provide reasonable insight into how the lamps' emissivity changes with respect to wavelength and temperature.

Along with emittance, objects intercepting radiation (known as irradiation) may also absorb, reflect, and transmit that irradiation as shown in **Figure 7**.

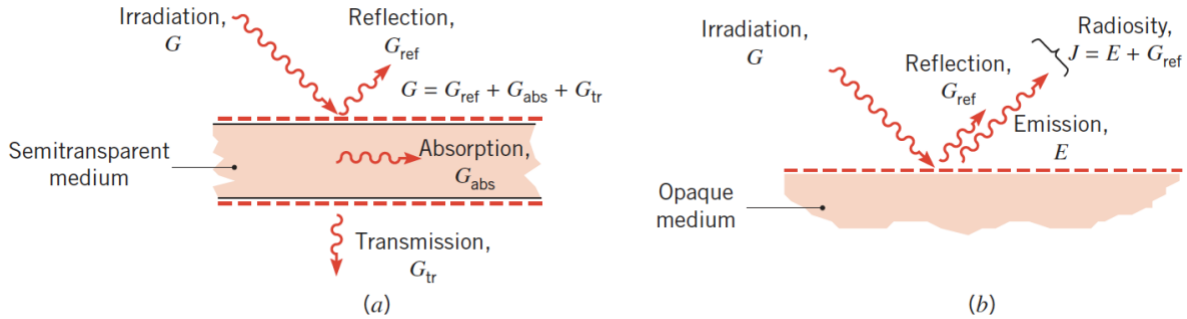

***Figure 7**: Radiation at a surface. (a) Reflection, absorption, and transmission of irradiation for a semitransparent medium. (b) The radiosity for an opaque medium [6].*

In **Figure 7**, G, E, and J represent rates of energy per unit area corresponding to irradiation, emission, and radiosity (total radiant energy leaving an object's surface), respectively. The difference between parts (a) and (b) in **Figure 7** is due to the nature of the object. Notably, opaque objects do not transmit radiation. The energy rates of reflection, absorption, and transmission can be compared to irradiation to obtain **Equation 4**.

$$\rho + \alpha + \tau = 1$$

***Equation 4**: The reflectivity (ρ), absorptivity (α), and transmissivity (τ) of an object being irradiated sum up to 1.*

Additionally, in opaque objects $\tau = 0$ such that the equation above simplifies. According to Kirchhoff's law, the total emissivity of a surface and the total absorptivity are equal when the surface irradiation is that of a blackbody emitter and is in thermal equilibrium with the source [9]. The assumptions associated with this law are very rigid as real objects are not blackbody emitters, and fundamentally absorptivity depends on irradiation whereas emissivity depends on the surface of the material intercepting the irradiation. Based on this relationship between emissivity and absorptivity, it can be inferred that they are proportional to each other. In addition to emissivity, absorptivity is another material property that is of importance for a lamp furnace. An object in the

furnace will absorb radiation and increase in temperature primarily based on the absorptivity of the object.

3.2: Previous Lamp Furnaces Designed for *in situ* Experimentation

The idea of a high-temperature lamp furnaces for heating samples has been reported in the literature. In a study by Sarin P. et al. a quadrupole lamp furnace for *in situ* powder XRD experiments was constructed. Their furnace utilizes four 150 W halogen lamps in a brass housing that are aligned such that their reflected light intercepts at the center of the furnace, and the distance from the lamp edge to the focused spot is ~19 mm [3]. A sample holder made from Pt20%Rh was fabricated to hold the powder samples in the furnace hot spot for temperature values up to 2125 K (~1850 °C) [3].

Sarin P. et al. results determined that the furnace maximum temperature measured via a Type B (Pt30%Rh–Pt6%Rh) thermocouple was 1773 K (1500 °C), but the furnace was able to heat a MgO reference sample to 2050 K (1775 °C) [3]. This discrepancy between thermocouple and sample temperature was attributed to two possible reasons. The thermocouple was approximately 2-3 mm above the sample and thus further from the hot spot, and the thermocouple is expected to have different absorption characteristics of the lamp's radiation compared to the sample [3]. The lamps used in their furnace are very similar to the ones in used in this work, so comparing the characterization results of the furnaces may be the most insightful into the differences between four and eight lamp furnace designs.

Another study that incorporates a lamp furnace for *in situ* experiments was conducted by H. A. Bale et al. in which μ-CT measurements are taken from a synchrotron source [2]. Their work sought out to obtain images of failure events in materials at high temperatures under mechanical loads. The lamp furnace they implemented is made up of six 150 W halogen lamps with the capability to enclose the furnace chamber for an inert environment (nitrogen gas). The temperature variation within their 5 mm "hot spot" is approximately 150 °C, [2]. Meaning that at 2.5 mm away from the center of the furnace, the temperature is 150 °C less than the peak temperature in the center. Temperature was measured using a Type C (W5%Rh-W26%Rh) thermocouple. They determined that the highest temperature achieved by the furnace was 1750 °C [2].

In their study, Bale et al. brought up that the temperature of the sample or thermocouple loaded into the furnace can be influenced by the object holding the sample/thermocouple in place. That object is effectively always cooler than the sample being radiatively heated such that it acts as a heat sink to transfer heat from the center of the furnace to the cooler end [2]. The characteristic measurements of the furnaces from these previous and additional studies as well as their lamp specifications are summarized in **Table 1**.

Study (Authors)	Number of 150W Lamps	Maximum Temperature (°C)	Maximum Sample Temperature (°C)	Hot Spot Size (mm)
Y. Wang et al.	2	N/A	350	~3
L. F. Siah et al.	4	1700	1400	~4
P. Sarin et al.	4	1500	1775	4
H. A. Bale et al.	6	1750	N/A	~3
C. Foster et al.	6	>1000	N/A	3.5

Table 1*: Key furnace characteristics of relevant lamp furnace studies. [2][3][4][5][6].*

The hot spot size in **Table 1** is defined as the region in the furnace where temperature change with respect to the maximum temperature does not exceed 20 °C. The hot spot dimensions from the H.

A. Bale et al. study was inferred based on their figures provided. Uncertainty in temperature measurements were not included in either study as they were determined to be insignificantly small.

3.3: Lamp Design

The OLF uses the International Light L6409-G 150 W lamps. These tungsten filament lamps are designed to reflect light such that most of it converges on a spot a focal distance away from the bulb [11]. The shape of the reflecting surface is ellipsoidal, as shown in **Figure 8**,

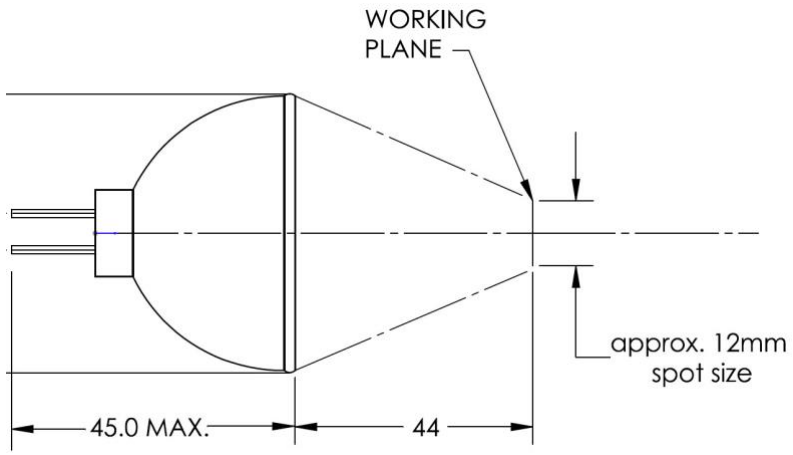

***Figure 8**: Reference drawing of G5.3 MR16 Halogen Reflector Lamp. Dimensions are in millimeters [11].*

and the reflector is coated in a gold film to better reflect infrared emissions. These lamps have an approximate focal distance of 44 mm, and an approximate focal spot length of 12 mm [11]. The distance from the lamp where the light is focused to, and the characteristic length of that focused spot are both important for the design of the furnace. The lamps are graded to run for 200 hours according to the manufacturer [11]. The furnace utilizing these lamps for high temperature heat

treatments needs to be able to operate to accommodate any necessarily low heating rates (i.e., to prevent thermal shock of samples in the furnace).

Heating tungsten to the high temperatures needed for furnace operation also makes it hot enough to sublimate, which leads to evaporation of the filament throughout the lifetime of the lamp. At that point, the evaporated tungsten particles are no longer contributing to the emission of light, and they tend to deposit on the bulb as a gray layer such that the light emitted is obstructed. To avoid sublimation of the filament, the lamp bulb is filled with halogen and xenon gas. The inert xenon gas suppresses the evaporation of the tungsten filament, which substantially lengthens the lifetime of the lamp [11]. Whereas the halogen gas (usually bromine) is there to react with any evaporated tungsten particles into tungsten bromide [11]. Tungsten bromide can move freely off the wall of the bulb when the bulb wall reaches a temperature of 250 °C, and it will eventually deposit back onto the filament (around 2500 °C, the bromine dissipates from the evaporated tungsten) [11]. This recovery cycle of tungsten does not perfectly capture all the tungsten evaporated back onto the filament, but it does significantly increase the lifetime of the lamp.

3.4: Octapole Lamp Furnace Design

The OLF is fashioned with features and design aspects to support mobile transportation of the furnace, open access for imaging, furnace cooling for ease of use, and more. The furnace is made of 6061-T6 aluminum alloy such that it is low cost and light weight [1]. The furnace along with the lamps embedded into it can be seen in **Figure 9**.

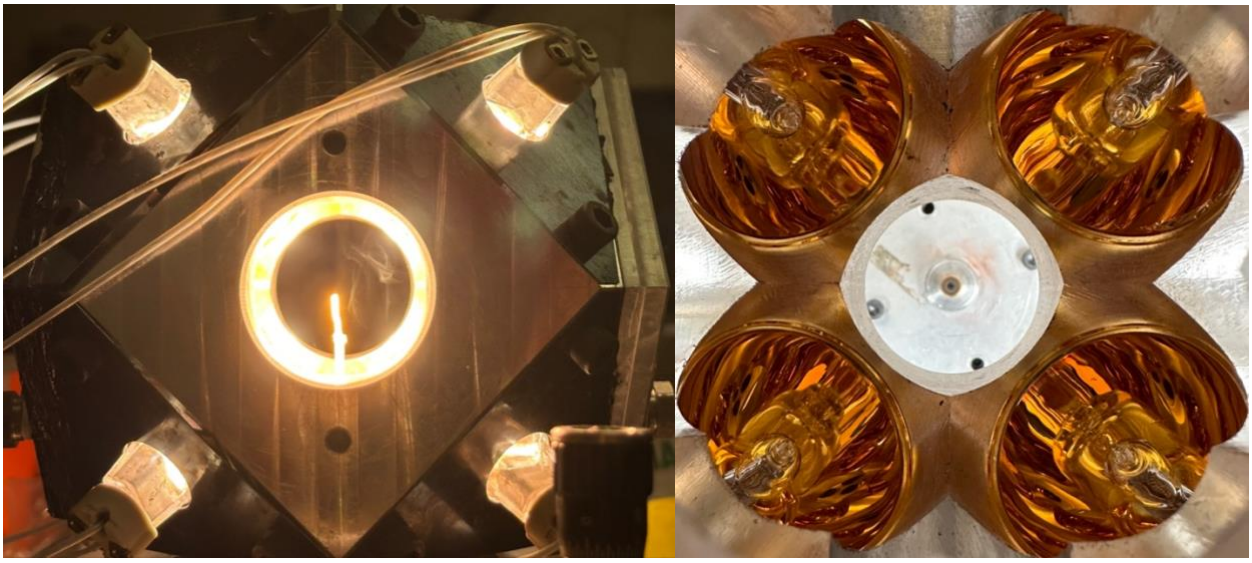

Figure 9*: (Left) Photo of powered OLF (side view). (Right) Photo of OLF looking into the bottom portion of the heating region from above.*

The center of the OLF does not contain anything to impede the light emitted by the lamps, and each side is equipped with threads to attach light-blocking pieces of metal because the light emitted can become bright enough to damage eyes. As seen in the corners of the left-side image in **Figure 9**, the lamps are fixed into the OLF via threaded inserts such that they can be easily removed for lamp replacement as needed. The OLF is also equipped with liquid-cooling channels along two sides of the furnace to help cool the furnace as the heat builds up in it during operation.

Additionally, the OLF is designed to be attached to a fixed support via a breadboard as shown **Figure 10** below.

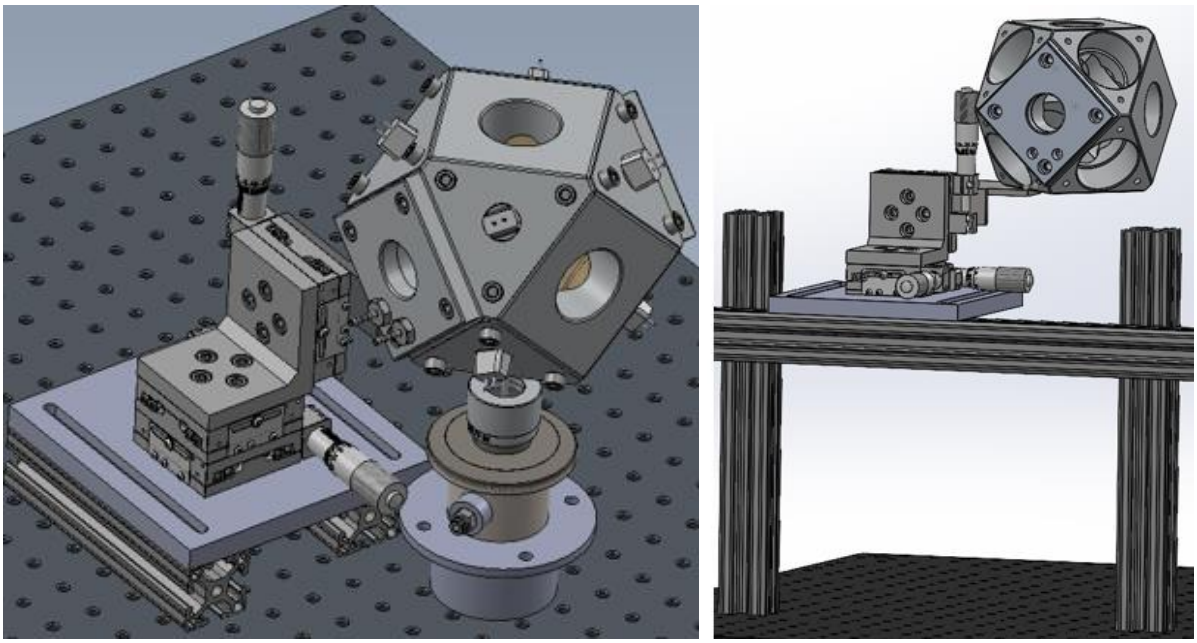

Figure 10*: (Left) OLF CAD schematic for table-top lab use. (Right) OLF CAD schematic for setup at beamline [1].*

where the left image is of the furnace setup for table-top lab usage and the right image described the furnace setup for use at a synchrotron source in which a large, motorized sample holder is below the furnace. In addition to adjusting the position of the plate holding the OLF along the metal extrusions, three linear positioners are used to adjust the position of the OLF via turning dials for each Cartesian coordinate with a range +/–10 mm.

Chapter 4: Sample Preparation for OLF Characterization

In this chapter, the details of synthesis/fabrication of the samples heat treated in the OLF are disclosed. These samples originated from powder-form chemicals. The implementation of an inert chamber used for inert-gas heat treatment in the OLF is also explained.

4.1: Sample Fabrication

Samples for the OLF were prepared to be of small size and length to assist in a higher concentration of heat flux onto the sample, such that its temperature is uniform, while allowing enough material for μ-CT imaging. The ideal sample would be of cylindrical shape, have a diameter of 1 mm, and a length no more than 10 mm. The cylindrical shape is important for μ-CT imaging as the sample needs to be rotated up to 180°, so any deviation from the axis of rotation could potentially move the sample out of field of the X-rays path as it rotates. The samples prepared in this work are made from ceramic oxide powders. The desired form of sample was achieved by extruding a paste of the sample through a syringe tip of 1 mm size.

A paste was prepared using Al_2O_3 and CaO powder, mixed in a mortar and pestle with a hydroxyl methyl cellulose binder, Darvan dispersant, and DI water. The binder acts as a binding agent for the powders to effectively stick together in the slurry. The dispersant helps lower the viscosity of the slurry for enhanced dispersing of powders so clumps of powder don't form for easier mixing. The recipe of a typical batch of samples is comprised of 1000 mg of oxide powder, 50 mg of binder, ~2 drops of dispersant (via ~2 mm syringe tip), and ~4 drops of DI water. The extruded samples are left to air-dry such that they become firm and easier to handle as shown in **Figure 11**.

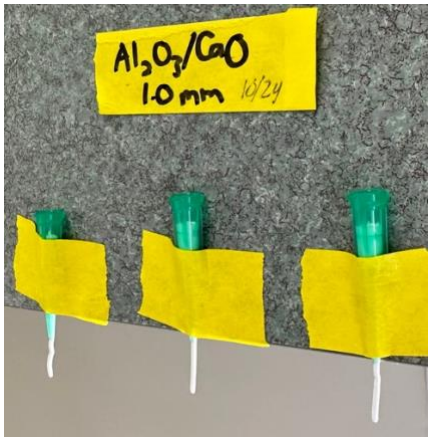

***Figure 11**: Extruded Al_2O_3/CaO samples during the air-drying step in sample preparation.*

At this point in the process, the samples are not a pure ceramic oxide mixture. The binder, dispersant, and any remaining water needs to be removed through a calcination step to ensure it is of pure phase. This is done by heat treating the samples in a ventilated furnace up to 600 °C (with a 12 hour dwell time, 5 °C/min ramp rate) such that the binder is removed from the sample as a gas. The process of the binder leaving the sample can cause deformations that typically result in the samples being even more brittle and difficult to handle. A secondary heat treatment step is then performed for sintering/reacting the sample above 1000 ˚C depending on the sample composition.

Some binary-mixture samples required additional preparation to achieve the desired phase. To better ensure any necessary high-temperature reactions occurred during heat treatments, the powders were pressed together into a pellet using a hand-press. This pellet was then heat treated at the desired temperature (with a 12 hour dwell time, 5 °C/min ramp rate) for the phase change to occur. The reacted pellet is crushed back into powder form in a mortar and pestle, and then the extruded sample preparation process is performed as previously described. After these heat treatments steps, the phase and composition of the samples are checked using XRD and XRF

techniques, respectively. A summary of the samples prepared in this work and their processing attributes is shown in **Table 2**.

Sample	Heat Treatment Temp. (°C)	Binder Mass Ratio (%)	Hand Pressed
Nb_2O_5/ZnO (32mol% Nb_2O_5)	1200	1.5	Yes
Al_2O_3/CaO (36.4mol% Al_2O_3)	1200	5	Yes
Nb_2O_5	1400	3	No
$BaTiO_3$	1500	3	No
SiO_2	1600	3	No

Table 2*: Summary of samples prepared for OLF characterization experiments and how they were processed. Heat Treatment Temp. refers to the temperature the sample was treated at after the calcination step occurred, and Binder Mass Ratio refers to the ratio of binder to sample mass used in the slurry initially prepared.*

In **Table 2**, binder to sample mass ratio was determined based on ease of handling samples during preparation while keeping the binder content of the mixture relatively low (<10%) to avoid breakage of samples during the calcination step.

4.2: Sample Holding

The samples prepared for the OLF need to be held in place inside the furnace for proper heating. Any sample holder will effectively block radiation from the lamps to the sample, so minimizing the size of the sample holder is important for the effectiveness of the furnace. Ceramic alumina tubes (of 1 mm inner diameter) were used to hold samples in place while being able to reach the center of the OLF. An adhesive was needed to secure the sample to the tube, so Al_2O_3 and ZrO_2 paste were both used because of their high melting points (2070 °C and 2715 °C, respectively) [14][15]. Very small amounts of paste were used because even though the paste would not melt,

the paste does dry out and can move the sample slightly while the furnace is on. A representative image of a sample being held by an alumina tube and alumina paste is shown in **Figure 12**.

***Figure 12**: Photo of a sample held using an Al_2O_3 tube and ceramic paste adhesive.*

In **Figure 12**, the alumina tube is being clamped in a collet secured to an aluminum base plate for stabilization.

4.3: Inert Chamber for Pyrolysis Capability in OLF

An inert chamber was constructed to provide a closed environment specifically for samples to be pyrolyzed in the OLF without any concern of reaction with the environment (i.e., oxidation). The portion of the chamber encasing the sample would ideally transmit any radiation from the lamps so that no heat flux is taken away from the sample. A quartz-silica tube was used to aspire to this effect, and preliminary measurements determined it did not significantly reduce the temperatures measured inside the OLF. The inert chamber was constructed to fit inside and reach the hot spot from the open holes on the sides of the OLF as shown in the **Figure 13**.

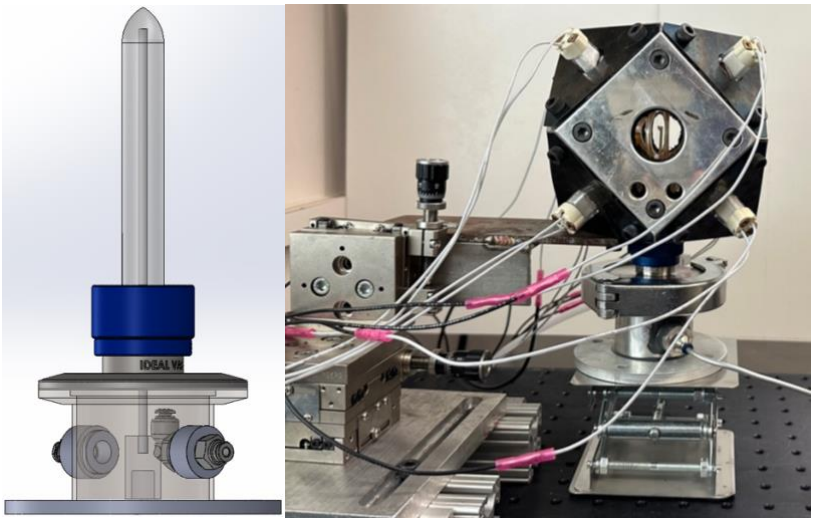

Figure 13*: (Left) Inert chamber CAD schematic [1]. (Right) Experimental setup with inert chamber implementation.*

As seen in **Figure 13** on the left, there are two ports for gas streams to be attached to. One for the inlet inert gas to flow up into the chamber, and another for the exiting gas to pass through. In the right-side image of **Figure 13**, the inert chamber is shown inside of the OLF with a clamped O-ring preventing the gases to escape from the seams of the chamber. The inert gas being flowed in this work was helium with the intention that its low density compared to air would allow the helium to easily rise into the chamber and surround the sample. An adjustable stand is used to vary height of the chamber inside the furnace for aligning samples. An additional port was added to place a thermocouple inside of the chamber as well. Advantageously, the inert chamber helps the temperature measurements stabilize as the gas trapped in the chamber can't escape and cause any slight cooling effects around the thermocouple.

Chapter 5: Octapole Lamp Furnace Characterization

In this chapter, the work for characterizing the OLF in the efforts of answering the technical questions posed in this thesis is showcased. The maximum temperature of the OLF is investigated and addressed from two perspectives. One from the thermocouple measurement of temperature, and the other from reaching the melting point temperature of a sample by melting it. The temperature gradient throughout the furnace is measured to unveil the dimensions of the hot spot of the furnace. This property is derived from the temperature profiles of the OLF in multiple directions.

5.1: Temperature Measurement Methodology

Measuring temperature inside of the OLF is not as simple as conventional furnaces. The source of heat is optically focused radiation, so there is a clear temperature gradient across the distance inside of the furnace. Typically, thermocouples are a convenient sensor for measuring temperature, but getting the thermocouple into the furnace raises a few concerns. First the thermocouple would ideally be in physical contact with the sample, and although the thermocouple junction from which the measurement is taken from is small, the samples used in the furnace are of 1 mm scale, so concealing the thermocouple from the irradiation of the furnace and having contact to the sample proves very difficult to achieve. Pyrometers on the other hand are a convenient instrument to measure temperature inside the OLF without needing to be inside of the furnace. The pyrometer measures temperature based on the emitted light of the sample while it is being irradiated/heated.

5.1.1: Pyrometer Measurements

The pyrometer employed in this work is an optical pyrometer, which raises concerns for this experimental setup. Optical pyrometers measure temperature by comparing the visible light emitted from the sample to a powered tungsten filament while accounting for the emissivity of the sample. Interference of the visible light emitted by the lamps occurred since the optical pyrometer operates in the red-light regime (~650 nm). This means that visible light is reflected by the sample into the pyrometer and affects the measurement of temperature. Upon preliminary measurements, the optical pyrometer was determined to be unreliable in measuring temperature as the temperature measured of a known sample was significantly above (hundreds of degrees) its melting point without any melting occurring in the sample. A representative data set showcasing this offset in temperature is shown in **Figure A1** of the appendix. Additionally, determining a correction for the pyrometer proved to be more difficult to achieve than anticipated since the interference of the lamps vary with their power as well as the choice of sample having its own reflectivity of radiation. Interestingly, the interference of the lamps should not apply to temperature gradients measured because they are performed at a constant power and sample. The pyrometer-measured temperature gradients are shown in **Figure A2** of the appendix.

5.1.2: Thermocouple Measurements

Type K (Ni10%Cr-Ni2%Al2%Mn1%Si) and Type B (Pt30%Rh–Pt6%Rh) thermocouples were used in this work to measure temperature inside the OLF. These thermocouples measure temperature between the ranges of –200-1250 °C and 0-1700 °C, respectively. Ceramic alumina tubes with two ~0.5 mm inner diameter holes were used to run each end of the thermocouples through so that the thermocouple would be held in place in the OLF. Many ways of incorporating

the thermocouple to measure the temperature of a sample were tested. Ultimately, using the thermocouple itself as the sample being heated proved to be the most stable setup as shown in **Figure 14**.

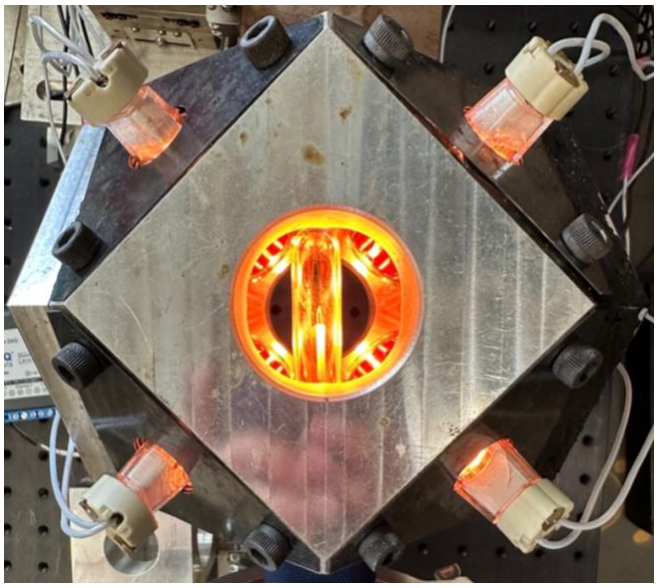

Figure 14*: Experimental setup for measuring temperature of the furnace using a thermocouple. Note that the inert chamber is being used in this image.*

As seen in **Figure 14**, the junction of the thermocouple is exposed to the irradiation with the alumina tube base holding it up. The quartz tube shown encasing the thermocouple is part of the inert-gas environment chamber. For measuring temperature while changing position of the thermocouple inside the OLF, an adjustable stand was used to change the height of the thermocouple and a ruler was used to measure distance inside the furnace. It was observed while adjusting the height of the thermocouple, there was clear interference of the thermocouple-holder transferring heat to the thermocouple via the temperatures measured (higher temperatures when the thermocouple junction was further from the center). Side-holding the thermocouple for these height measurements was used to remove that effect by keeping the interference of the thermocouple-holder as a constant as the height changed.

5.2: Maximum Temperature Results/Discussion

5.2.1: Temperature Measurement

The temperature of a Type B thermocouple was measured by placing the junction of the thermocouple in the center of the OLF as shown in **Figure 14**. The maximum temperature of the furnace corresponds to the temperature in the hot spot while the furnace is running at maximum power. Temperature measurements were taken as OLF power was increased to its maximum power as seen in **Figure 15**.

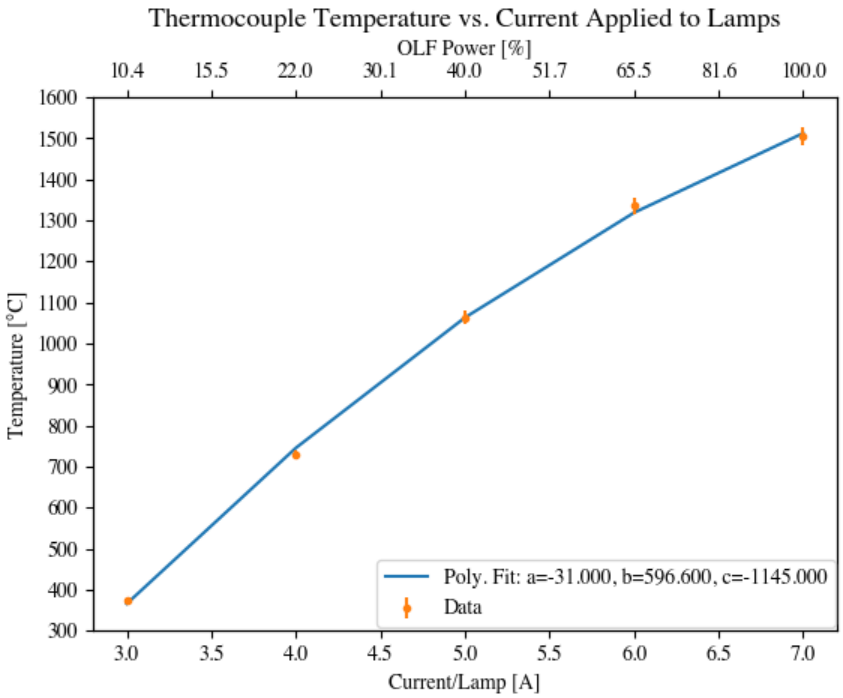

***Figure 15**: Thermocouple temperature vs. current applied per lamp in the OLF. Corresponding OLF power percent values are displayed in the top x-axis.*

Current is chosen as the independent variable because it is a setting that is user-inputted on the power supplies powering the OLF. Although the lamps begin to emit light at 2 A, the Type B thermocouple is not reliable at measuring the corresponding low temperature because of the small

voltage differences that correspond to low temperatures [16]. The maximum temperature value measured at maximum power of the OLF is 1504±23 °C. The uncertainty in this measurement comes from the uncertainty of the thermocouple (±1.5%) [17]. A best-fit polynomial was made to determine a functional form of the temperature in the furnace. This resulted in a parabola with constants as shown in the plot legend of **Figure 15**.

5.2.2: Sample Melting Point

The maximum temperature of the OLF was also determined from the perspective of melting prepared samples as proof of reaching their melting point temperature. Photos and video footage of the samples before, during, and after melting were captured to provide evidence of melting occurring. Before and after photos are included of a representative sample in **Figure 16**.

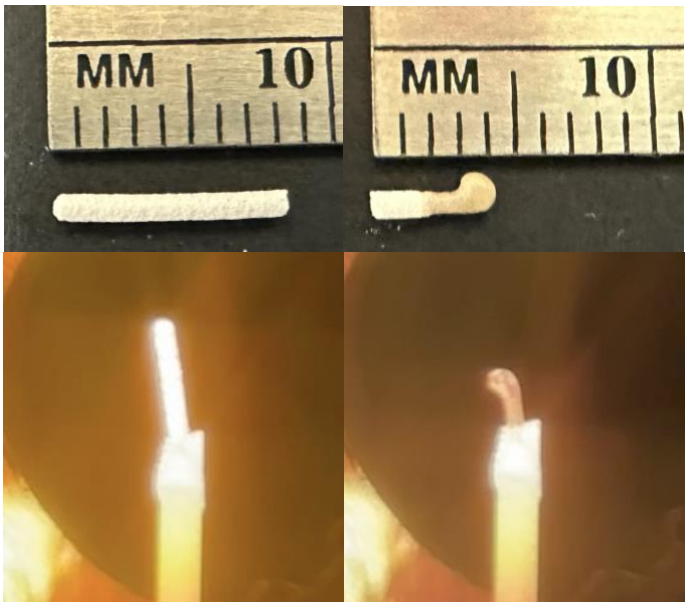

***Figure 16**: $BaTiO_3$ sample melting in OLF. (Left) Before melting. (Right) After melting. Photos taken during OLF operation utilized welding glass to filter the extremely bright light emitting from the furnace.*

The $BaTiO_3$ sample undergoes a solid to liquid phase change as evident by melt pool formation as well as the change in reflectivity/emissivity of the sample shown on the right side of **Figure 16**. The melt pool formation refers to the part of the sample that is seemingly melting and building a "pool" of itself as the transition from solid to liquid state results in the weight of the melting portion to fall on itself since the liquid has no fixed shape. The surface tension of the melt pool contributes to it forming a spherical shape because that shape minimizes surface area as well as the surface energy of the melt pool. The change in reflectivity/emissivity is inferred by the observation that the way the sample is reflecting/emitting light changes as it appears darker. Data on other ceramic samples tested in the OLF are summarized in **Table 3** below.

Sample	Melting Point (°C)	Melt Current (A/lamp)	OLF Power Applied (%)	Length of Sample Melted (mm)
Nb_2O_5/ZnO (32mol% Nb_2O_5)	1285±6	6.5	81.6	3.5±0.5
Al_2O_3/CaO (36.4mol% Al_2O_3)	1371±11	N/A	N/A	N/A
Nb_2O_5	1512	5.7	56.9	6±0.5
$BaTiO_3$	1625	6	65.5	7±0.5
SiO_2	1710	N/A	N/A	N/A

Table 3*: Representative samples tested for melting in the OLF in order of increasing melting point. Melt current indicates the current setting from which the sample melted, and OLF power applied refers to the corresponding furnace power values associated with the melt currents. Uncertainties of melting points in binary-system samples based on reported values, and uncertainty in length of sample based on measurements from a ruler [18][19][20][21].*

In **Table 3**, the furnace settings used to melt samples as well as the lengths of the samples are included. Phase diagrams of the binary-mixture samples prepared are included in **Figure A3** and **Figure A4** of the appendix. Samples with "N/A" did not melt in the OLF at maximum power. The confirmation of melting $BaTiO_3$ in the OLF as the highest melting temperature achieved in the

furnace is the determined answer to question 1 of the technical questions presented in the thesis objectives. This conclusion is based on being unable to melt SiO_2 samples in the OLF, but other samples may be better compatible with the OLF and worth investigating such that the maximum sample temperature may be higher. As displayed in the phenomena related to **Figure 4** and **Figure 7**, the OLF is heating samples via radiation, and the sample's own reflectivity, absorptivity/emissivity, and transmittivity determine how it interacts with the most visible and infrared radiation the lamps emit. The Al_2O_3/CaO and SiO_2 samples may not be as compatible with the OLF as the other meltable samples.

The length of the sample proved to be an important determining factor in how much power was needed to melt it. The main hypothesis was that shorter samples mounted in the sample holders would allow more of the sample holder to be closer to or in the hot spot which would interfere with the radiation directly hitting the sample. This would affect the power of OLF needed to melt the sample as not all the energy would be absorbed by the sample such that more power would be needed to melt the sample. However, larger samples in general are expected to require more energy to increase their temperature since there is more material to absorb energy than with smaller samples. Adjusting the sample length provided insight to these claims. Increasing the sample length of Nb_2O_5 from 3.5 mm to 6 mm decreased the power necessary to melt it and increasing the sample length of $BaTiO_3$ from 7 mm to 10 mm increased the power necessary to melt it. These observations suggest that there is an ideal range of sample lengths for the OLF, and it would be in between 6-7 mm based on these preliminary investigations.

5.3: Hot Spot Dimensions Results/Discussion

Understanding how the temperature changes inside of the furnace is important for determining the size of the hot spot. The hot spot is the region of the furnace where the highest amount of energy/heat flux from the lamps is irradiated to the sample. In accordance with the work of P. Sarin et al., the hot spot is defined as the region of the furnace where temperature gradients are less than 20 °C [3]. Temperature measurements were taken using Type K and Type B thermocouples while varying the position of the sample within the furnace in 3 directions as shown in **Figure 17**.

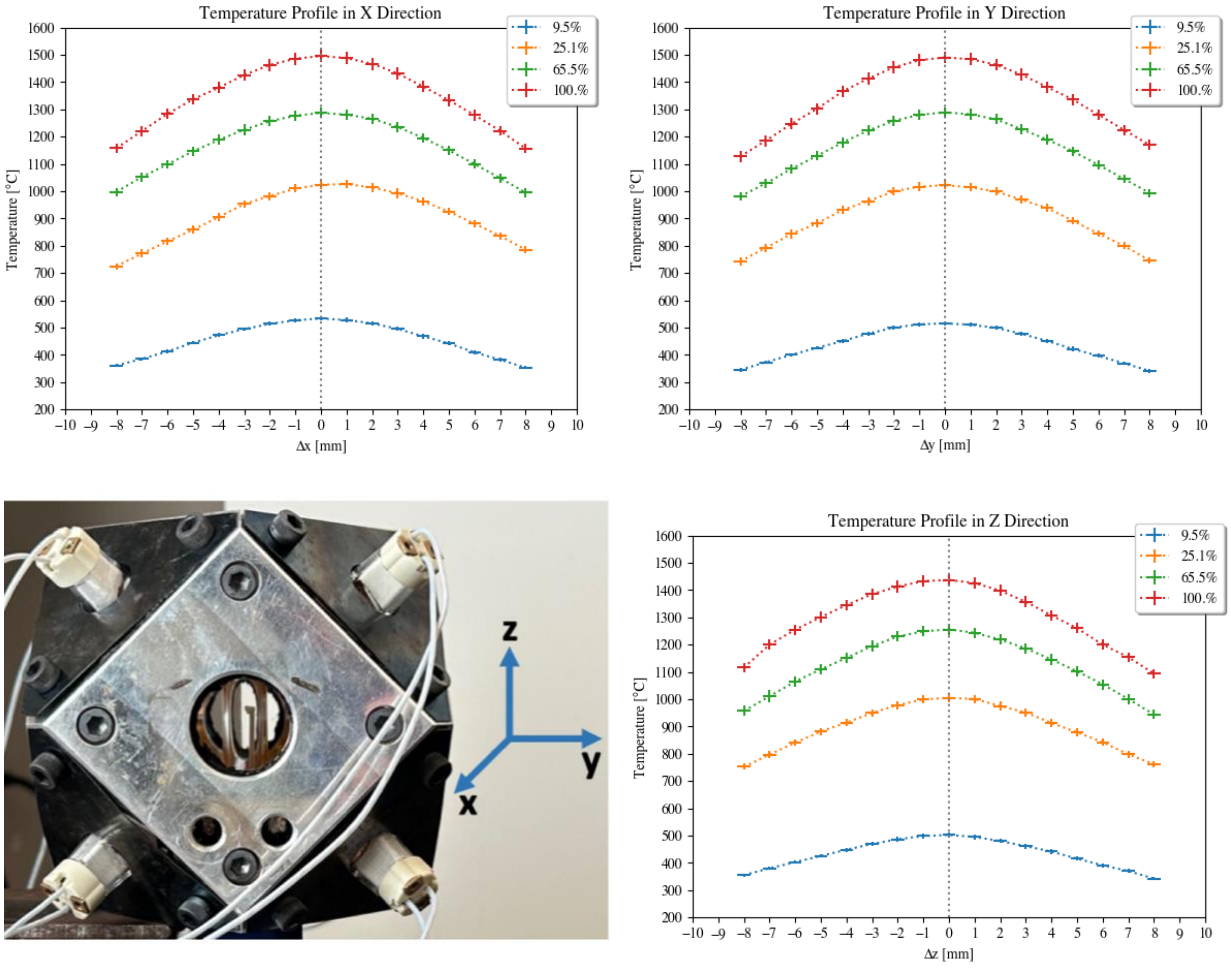

***Figure 17**: Temperature profile in each Cartesian direction inside the OLF based on three sets of data for each power setting. (Top Left) X-axis profile. (Top Right) Y-axis profile. (Bottom Left)*

Coordinate system reference for OLF. (Bottom Right) Z-axis profile. Legend in terms of percentage of power of the OLF. Error bars refer to the standard deviation of temperature measurements, and the uncertainties of the thermocouple and ruler used for measurements.

In **Figure 17**, the geometric center of the OLF was chosen as a reference point where the displacement (Δ) is equal to zero. In each coordinate and for each percentage of OLF power, the temperature decreases from the zero point. The symmetry about the zero point suggests that the geometric center of the OLF is where the hot spot is located, but there are slight deviations primarily in the z-direction profiles as well as the 25.1% power x-direction profile.

Deviations in the symmetry of the temperature profiles may be caused by the alignment of the lamps affecting the focusing of the radiation, and they may be caused by the method used to take measurements. The z-direction measurements were cumbersome to obtain because an adjustable stand was used to adjust the height of the sample holder side-holding the thermocouple in the OLF. The stand wouldn't raise the plate exactly parallel to the z-axis, which would introduce error in the position and therefore temperatures measured. For explicitly determining the size of the OLF's hot spot, data was consolidated from **Figure 17** into **Table 4** below.

OLF Power (%)	**Change in Temperature = 20 °C**			**Hot Spot Dimensions: X-Y-Z (mm)**
	X-Direction Bounds (mm)	**Y-Direction Bounds (mm)**	**Z-Direction Bounds (mm)**	
9.5	–2, +2.05	–2.15, +2.1	–2.2, +1.9	4.05 - 4.25 - 4.10
25.1	–1.1, +2.3	–1.8, +1.8	–1.7, +1.65	3.40 - 3.60 - 3.35
65.5	–1.45, +1.8	–1.5, +1.7	–1.6, +1.3	3.25 - 3.20 - 2.90
100	–1.5, +1.7	–1.4, +1.75	–1.75, +1.4	3.20 - 3.15 - 3.15

***Table 4**: Bounds of hot spot region in each direction at different OLF powers with culminating hot spot dimensions. Uncertainty in the measured bounds is ±0.5 mm.*

In **Table 4**, the hot spot dimensions are listed at different power settings. These dimensions are assigned to specific directions and do not assume the shape of the hot spot. As expected by the slight deviations in symmetry observed in **Figure 17**, the bounds are not exactly symmetric about the zero point (the values would all be the same in the negative and positive direction otherwise). The low power OLF hot spot has a characteristic length of ~4 mm whereas the full power OLF hot spot has a characteristic length of ~3 mm. These values are very similar to previous lamp furnace referenced in **Table 1**. These sizes of the hot spot are determined to be the answer to question 2 of the technical questions posed in the thesis objectives.

It is pertinent to note that the uncertainty in the values of **Table 4** is significantly large such that the hot spot dimensions have low precision. Despite this, there is a trend observed that as the power of the OLF increases, the dimensions of the hot spot decreases. The power increase results in higher temperatures, and the energy required to sustain the peak temperature at 100% furnace power (~1500 °C) versus 10% (~500 °C) is larger because, generally, as solids increase in temperature their heat capacities increase as well. The increase in heat capacity affects how much heat is required to change the temperature as shown in **Equation 5**.

$$\mathrm{Q} = C_P m \Delta \mathrm{T}$$

Equation 5*: The heat (Q) required to change the temperature of an object equals to the specific heat capacity (C_P) multiplied by the mass (m) and change in temperature (ΔT).*

Comparing **Equation 5** for the 10% and 100% power settings with the assumption that the heat capacity at 100% power is greater than that of 10% results in

$$\frac{\mathrm{Q}_{10\%}}{\mathrm{Q}_{100\%}} = \frac{C_{P_{10\%}} m \Delta \mathrm{T}}{C_{P_{100\%}} m \Delta \mathrm{T}} \rightarrow \mathrm{Q}_{100\%} = \left(\frac{C_{P_{100\%}}}{C_{P_{10\%}}}\right) \mathrm{Q}_{10\%} \rightarrow \mathrm{Q}_{100\%} > \mathrm{Q}_{10\%}$$

such that the heat required to change the temperature by 20 °C at 100% is larger than when at 10% OLF power. This could account for why the temperature change defining the hot spot is occurring at shorter lengths as the power of the OLF increases (more concentration/overlap of heat from the lamps is needed, and that occurs over a smaller volume).

5.4: OLF Characterization Conclusion

The answers to the two technical questions proposed in the thesis objectives were answered based on the OLF temperature data collected and evidence of melting samples in the OLF. The maximum temperature of the OLF was determined to be 1504±23 °C, and the highest melting point material melted in the OLF was $BaTiO_3$ (MP: 1625 °C). The characteristic length of the OLF hot spot was determined to be ~3 mm at maximum power and ~4 mm at lower power settings. Understanding these properties of the furnace informs the capabilities of it for pyrolysis experiments coupled with μ-CT measurements.

Chapter 6: Pyrolysis Experiments for *in situ* μ-CT

In this chapter, the OLF is assessed for whether it can pyrolyze a preceramic polymer sample into a ceramic while keeping the sample intact throughout its heat treatment (avoiding thermal shock of the sample).

6.1: Pyrolysis in OLF Methodology

The effectiveness of the OLF to pyrolyze a material while accounting for thermal shock of the material as it pyrolyzes was assessed using polycarbosilane SMP-10 samples. These samples are Si-C polymer precursors that go through an off-gassing process as they are pyrolyzed. Mass loss data of SMP-10 as it is pyrolyzed is shown in **Figure 18** from work done by Thomas K. et al. [22].

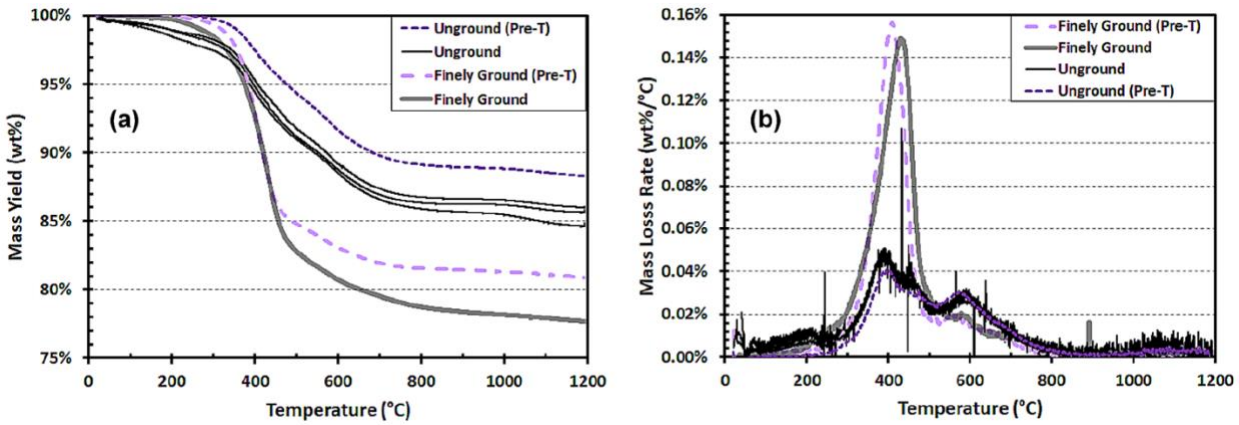

***Figure 18**: (a) Mass yield and (b) mass loss rate for vacuum cured SMP-10 in the form of a single piece and a finely ground powder. Samples from both received and pretreated SMP-10 was cured [22].*

Based on the mass yield data of SMP-10 shown in **Figure 18**, the temperature region where off-gassing occurs is around 200-800 °C. During this off-gassing process, the sample is more susceptible to cracking as gas forms and needs to escape.

A sample that undergoes thermal shock in the OLF would break into smaller pieces and expectedly be knocked off the sample holder which would ruin any *in situ* measurements being taken. Preventing thermal shock and failure from off-gassing requires heating the sample at a rate slow enough such that the gas escaping from the sample and deformations associated with it don't occur fast enough. The direct way of adjusting the OLF's heating rate is through the lamp power supplies. The power supplies use a digital interface through a computer for users to adjust the voltage/current of the lamps. The approach taken for testing the heating ramp rates to prevent thermal shock of SMP-10 samples was chosen to minimize the total time needed to reach the OLF's maximum power settings. Because the power supplies could support increases of current on the magnitude of 0.001 A, there was a wide range of ramp rates to consider for reaching the maximum power setting of 7 A/lamp [23]. Additionally, pycnometer measurements were taken of samples pre and post pyrolysis to quantitively confirm densification occurred as expected from pyrolyzing SMP-10.

6.2: OLF Ramp Rate for Pyrolysis Results/Discussion

Utilizing the inert-gas chamber constructed for pyrolysis experiments and thermocouples as a reference for the temperature inside the OLF, heat treatment experiments were performed to test different ramp rates of the furnace. The ramp rates investigated are summarized in **Table 5**.

OLF Ramp Up (A/lamp)	Dwell Time (min)	Uniform Ramp Rate	Thermal Shock Occurred
0.5	0.5	Yes	Yes
0.2	1	Yes	Yes
0.1	1	Yes	Yes
0.1	1	No	Yes
0.05	1	No	No

***Table 5**: Summary of the furnace ramp rates investigated for heating SMP-10 samples without achieving thermal shock of the sample.*

After multiple tests to determine a sufficient rate to heat the sample up to max OLF power, a ramp rate of 0.05 A/lamp-min was used during the off-gassing temperature region and a ramp rate of 0.1 A/lamp-min was used in other temperature regions. Repeated trials of these ramp rates ensured that no thermal shock of the samples occurred. A representative temperature profile used to investigate the ramp up rate of the furnace is included in **Figure 19**.

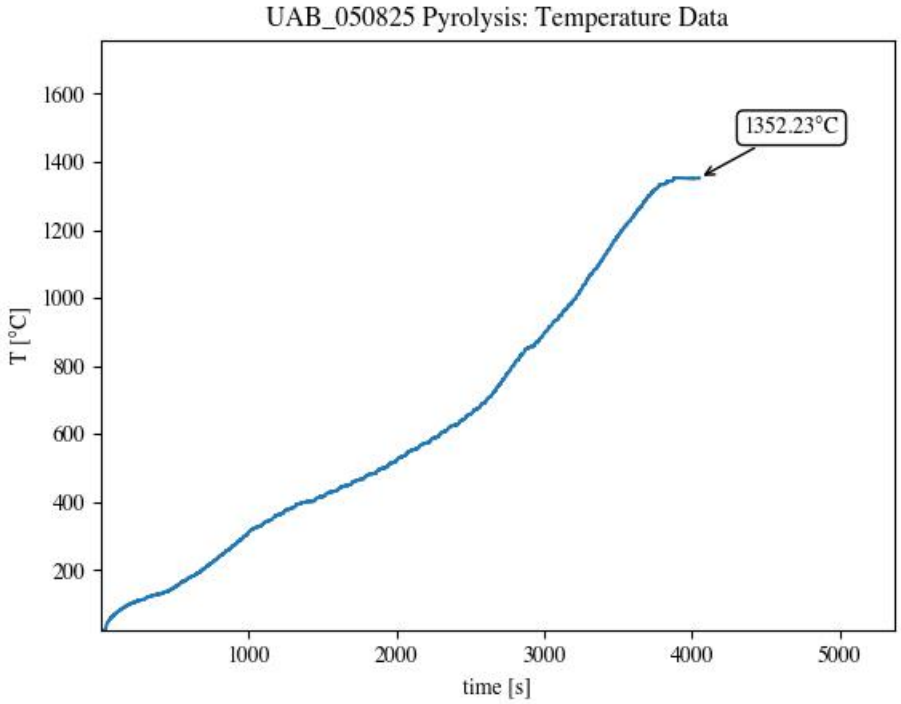

***Figure 19**: Temperature profile measured using Type B thermocouple placed 1 mm from SMP-10 sample. Error in temperature measurements were not included in order to emphasize the change of the slope.*

In **Figure 19**, it is apparent that the use of two ramp rates results in two distinct regions with the same increase of temperature (~300-700 °C region's slope is lower than the rest of temperature profile). The ramp rates used resulted in ~1 hour of OLF operation time to go from 0 to 100%

power, which could be shortened if faster ramp rates were investigated outside of the pyrolysis temperature region of SMP-10. Images of a representative sample of SMP-10 before and after heat treatment (using helium as the inert-gas) in the OLF are shown in **Figure 20**.

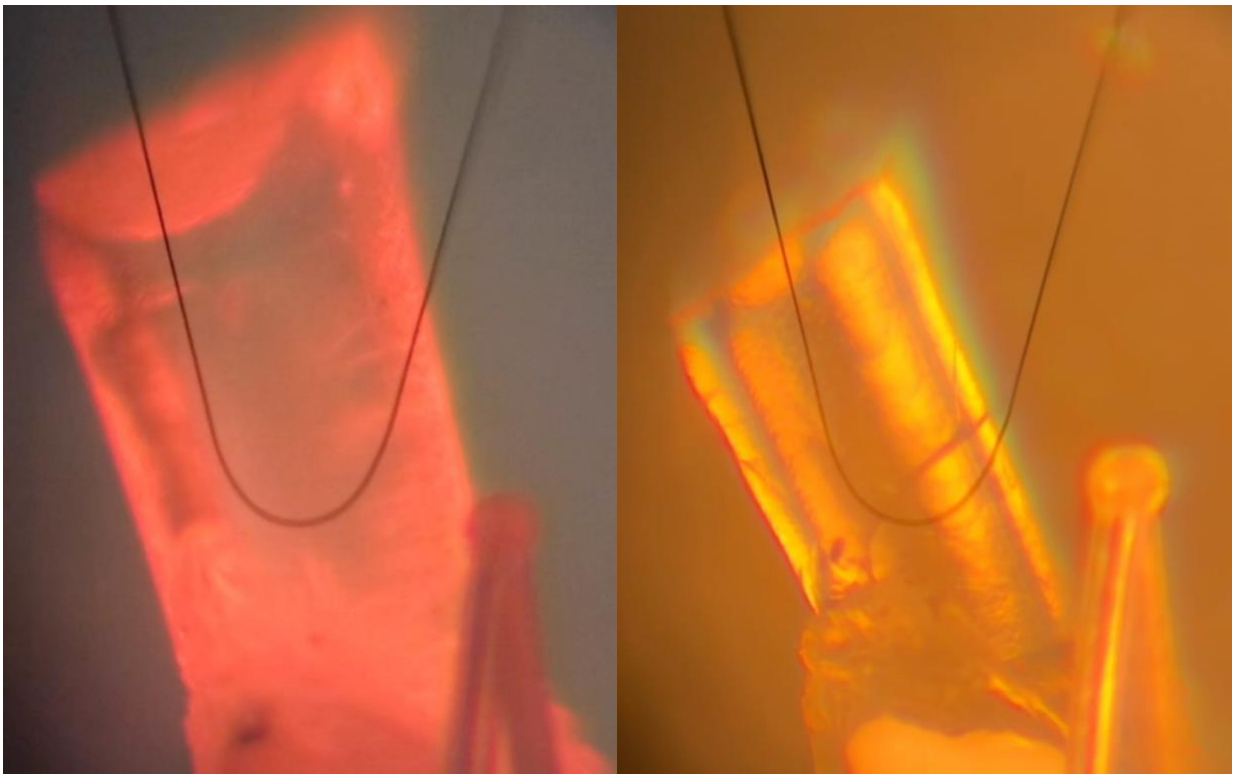

Figure 20*: (Left) Before pyrolyzing SMP-10 sample. (Right) After pyrolyzing SMP-10 sample in OLF under inert-gas conditions. Images taken from a video recording of the heat treatment of the sample (camera position and zoom-setting remained constant during the recording).*

Comparing the before and after images of **Figure 20** clearly shows evidence of pyrolysis and densification of the SMP-10 sample due to the decrease in volume of the sample as well as the decrease in translucency of the sample.

In addition to the visual evidence of pyrolysis occurring, density measurements were taken using a pycnometer before and after heat treatment in the OLF to validate whether densification through

the polymer conversion to ceramic process occurred. Representative data of heat treated SMP-10 samples are shown in **Table 6**.

Sample	Density Pre-Heating (g/cm^3)	Density Post-Heating (g/cm^3)
SMP-10 3mm	1.1083±0.0057	4.0428±0.0989
SMP-10 4mm	1.1083±0.0057	3.8767±0.1148

Table 6*: Density measurements of SMP-10 samples pre and post heat treatment to the max power of the OLF. Each pycnometer measurement includes the standard deviation of that measurement.*

In **Table 6**, the density of SMP-10 samples increases approximately fourfold from heat treatment to maximum power in the OLF. Based on the successful runs of pyrolyzing SMP-10 in the OLF with the inert-gas chamber, the OLF is compatible with *in situ* μ-CT experiments for imaging the densification process of SMP-10.

6.3: Pyrolysis Experiment Conclusion

The answers to questions 1 and 2 from the thesis objectives were determined from these pyrolysis experiments in the OLF. A ramp rate of 0.05 A/lamp-min and 0.1 A/lamp-min used during and outside of the off-gassing regime of SMP-10, respectively, was determined to successfully pyrolyze SMP-10 in the OLF without inducing thermal shock of the samples. The inert-gas chamber was successful as an environment for pyrolysis of SMP-10 inside the OLF. Density measurements pre and post heat treatment of SMP-10 in the OLF provides quantitative evidence of densification occurring via pyrolysis (sample density increased by a factor of four).

Chapter 7: Conclusion and Future Work

7.1: Conclusion

This work investigated the capabilities of the OLF for effectively heating samples to be coupled with μ-CT experimentation. These capabilities include the maximum temperature of the furnace, size of the hottest spot in the furnace, and compatibility with pyrolyzing polymer precursors into PDCs. The objectives of this work were fulfilled by answering the following questions:

1. What is the OLF's maximum temperature?
2. What is the size of the OLF's hot spot?
3. Can the OLF effectively heat samples that require low ramp rates to prevent thermal shock?
4. Can the OLF pyrolyze PDC samples using an inert-gas environment chamber?

Analysis of the data collected for the maximum temperature of the OLF determined the maximum temperature of a Type B thermocouple in the OLF was 1504±23 °C, and that the OLF was able to melt $BaTiO_3$ as proof of achieving its melting point temperature of 1625 °C. The size of the hot spot (the region with <20 °C temperature change) of the OLF at max power was determined to be ~3 mm in each x-y-z coordinate with respect to the geometric center of the furnace. The OLF was successful in heating SMP-10 samples up to full power operation with ramp rates that did not cause thermal shock of the samples (0.05 A/lamp-min). The OLF was also successful in pyrolyzing SMP-10 samples with the integration of an inert-gas environment chamber inside of the OLF. The integration of the quartz-tube encasing the sample inside of the OLF did not significantly impact how hot the sample was able to get when compared to heating with no chamber. These findings demonstrate that the OLF is feasible for *in situ* experiments.

7.2: Future Work

The results obtained from this work suggest that temperature quantification of a radiative-power-source furnace is not as straightforward as conventional high temperature furnaces. Another method of better quantifying the OLF's energy output is by measuring the amount of energy emitted into the hot spot. A broadband thermopile is a device that has similar sensor technology to a thermocouple but is more compatible with non-contact measuring and absorbs more infrared radiation, so it should be sufficient in determining the maximum power inside the OLF.

Another potential method of better quantifying the maximum temperature inside the OLF is using an infrared pyrometer system. The infrared pyrometer measures temperature based on the infrared light emitted by the sample as it is being heated. Rapid switching and spectral measurement techniques can be used to avoid reflected light from the lamps from interfering with the measurement of the sample. These measurements can be done by pyrometer systems that can distinguish between reflected and emitted light.

Further investigation can be done on the precision of the hot spot dimensions as well as determining the shape of the hot spot. It can be inferred that from the radially emitting sources that the lamps are that the overlap of their hot spots would result in a spherical/conical volume, but the region of that volume that falls under the definition of the hot spot used in this work may be only a subset of it. Radial temperature measurements may be achievable with reconsiderations to the experimental setup done in this work.

References

[1] K. Tanaka et al., *Design and Manufacture of Optical Lamp Furnaces*, M.S. Thesis, University of California, Davis, 2025.

[2] Bale, H. A. et al., "Real-time quantitative imaging of failure events in materials under load at temperatures above 1,600°C," *Nature Materials*, 2012.

[3] P. Sarin, W. Yoon, K. Jurkschat et al., "Quadrupole lamp furnace for high temperature (up to 2050K) synchrotron powder x-ray diffraction studies in air in reflection geometry," *Review of Scientific Instruments*, 2006.

[4] Wang, Y., Denney, J. J., Corrao, A. A., Huang, G., Zhang, M., Soundararajan, P., Montiel, D., Thornton, K., & Khalifah, P. G. (2021). Sample environment effects on synchrotron-measured temperature profiles in an approximant of optical floating zone crystal growth. Journal of Crystal Growth, 574. https://doi.org/10.1016/j.jcrysgro.2021.126331.

[5] Siah, L. F., Kriven, W. M., & Schneider, J. (2005). In situ, high-temperature, synchrotron, powder diffraction studies of oxide systems in air, using a thermal-image furnace. Measurement Science and Technology, 16(6). https://doi.org/10.1088/0957-0233/16/6/008.

[6] Foster, C. W., Oruganti, S., & Panerai, F. (2023). Real-time quantitative imaging of RTV silicone pyrolysis. Polymer Degradation and Stability, 214. https://doi.org/10.1016/j.polymdegradstab.2023.110403.

[7] Colombo, P., Mera, G., Riedel, R. and Sorarù, G.D. (2010), Polymer-Derived Ceramics: 40 Years of Research and Innovation in Advanced Ceramics. Journal of the American Ceramic Society, 93: 1805-1837. https://doi.org/10.1111/j.1551-2916.2010.03876.x.

[8] Chaudhary, R. P., Parameswaran, C., Idrees, M., Rasaki, A. S., Liu, C., Chen, Z., & Colombo, P. (2022). Additive manufacturing of polymer-derived ceramics: Materials, technologies, properties and potential applications. In Progress in Materials Science (Vol. 128). https://doi.org/10.1016/j.pmatsci.2022.100969.

[9] Bergman, T. L., Lavine, S.A., Incropera, F.P. and Dewitt, D.P. (2011) Fundamentals of Heat and Mass Transfer. 7th Edition, John Wiley & Sons, Hoboken.

[10] Marr, J. M., & Wilkin, F. P. (2012). A better presentation of Planck's radiation law. *American Journal of Physics*, *80*(5), 399–405. https://doi.org/10.1119/1.3696974.

[11] "ILT Light Sources Catalog," International Light Technologies.

[12] de Izarra, C., & Gitton, J.-M. (2010). Calibration and temperature profile of a tungsten filament lamp. European Journal of Physics, 31(4). https://doi.org/10.1088/0143-0807/31/4/022

[13] Dmitriev, V. D., & Kholopov, G. K. (1965). Radiant emissivity of tungsten in the infrared region of the spectrum. Journal of Applied Spectroscopy, 2(6). https://doi.org/10.1007/BF00655100.

[14] Mao, H., Selleby, M., & Sundman, B. (2004). A re-evaluation of the liquid phases in the CaO-Al2O3 and MgO-Al2O3 systems. Calphad: Computer Coupling of Phase Diagrams and Thermochemistry, 28(3). https://doi.org/10.1016/j.calphad.2004.09.001.

[15] Zirconium Oxide Properties. American Elements. CAS: 1314-23-4.

[16] Revised Thermocouple Reference Tables – Type B Reference Tables, N.I.S.T. Monograph 175, Revised to ITS-90.

[17] DI-245 User's Manual. Revision G. DATAQ Instruments, Inc.

[18] McCormack, S. J., Tamalonis, A., Weber, R. J. K., & Kriven, W. M. (2019). Temperature gradients for thermophysical and thermochemical property measurements to 3000 °C for an

aerodynamically levitated spheroid. Review of Scientific Instruments, 90(1). https://doi.org/10.1063/1.5055738.

[19] A. A. Ballman and H. Brown, J. Cryst. Growth, Fig. 92-007—System ZnO-Nb2O5. 41 [1] 36-40 (1977).

[20] Barium Titanate Properties. American Elements. CAS: 12047-27-7.

[21] Silicon (IV) oxide, amorphous, 99.5% purity, Alfa Aesar Chemicals.

[22] Key, T. S., Patel, D. K., Wilks, G. B., & Cinibulk, M. K. (2021). Modeling the pyrolysis of preceramic polymers: A kinetic study of the polycarbosilane SMP-10. Journal of the European Ceramic Society, 41(13). https://doi.org/10.1016/j.jeurceramsoc.2021.06.011.

[23] Series 2260B Programmable DC Power Supplies Datasheet. Keithley, A Tektronix Company.

Appendix

A.1: Pyrometer OLF Characterization Data

A.1.1: Pyrometer Sample Temperature vs. Current in OLF

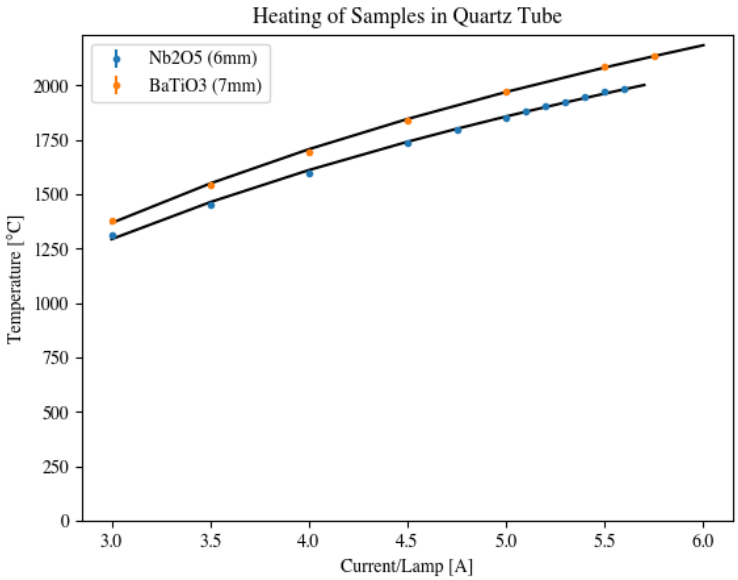

Figure A1*: Emissivity corrected pyrometer measures of samples heating in the OLF. Error bars in temperature determined by the uncertainty of the pyrometer.*

A.1.2: Pyrometer Temperature Gradient in the OLF

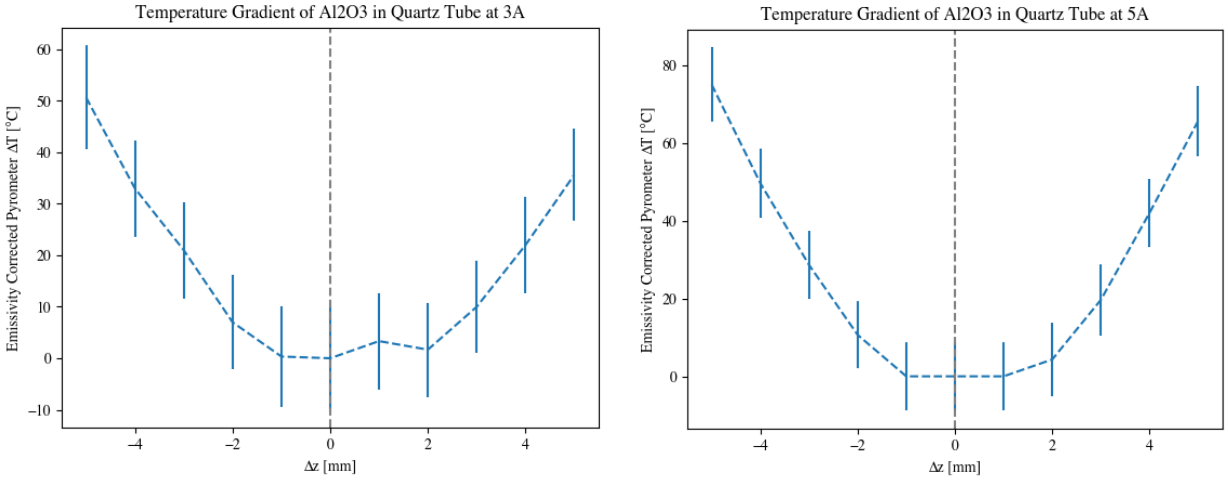

Figure A2*: Pyrometer temperature gradient profiles of the OLF about geometric center of Z-axis (emissivity of Al_2O_3 assumed to be 0.9). Error bars in temperature determined by the RSS of the standard deviation of three data sets and the uncertainty of the pyrometer.*

A.2: Phase Diagrams of Prepared Binary-Mixture Samples

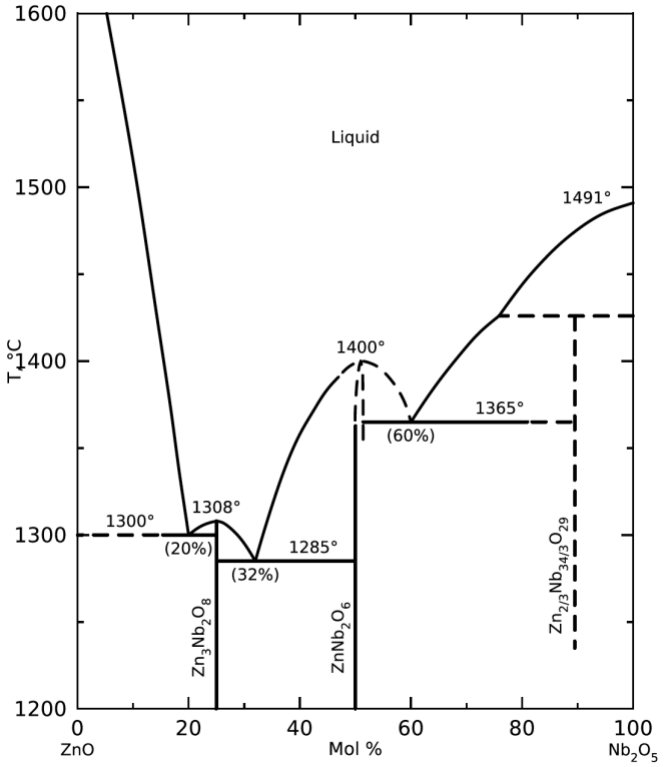

***Figure A3**: Nb_2O_5 and ZnO binary phase diagram [19].*

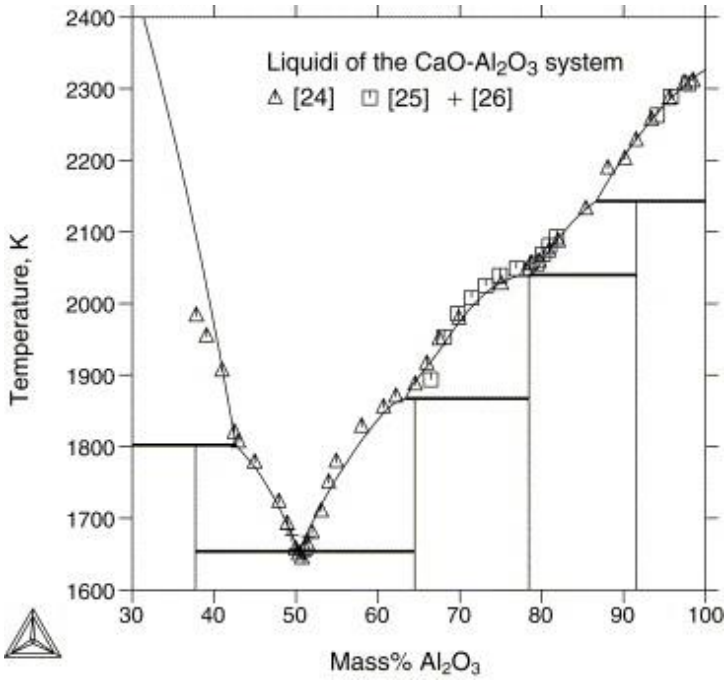

***Figure A4**: Al_2O_3 and CaO binary phase diagram [14].*